Macromolecules

ARTICLE

pubs.acs.org/Macromolecules

Construction and Validation of All-Atom Bulk-Phase Models of Amorphous Polymers Using the TIGER2/TIGER3 Empirical Sampling Method

Xianfeng Li,[†] N. Sanjeeva Murthy,[‡] and Robert A. Latour*[,†]

[†]Department of Bioengineering, Clemson University, Clemson, South Carolina 29634, United States

[‡]New Jersey Center for Biomaterials, Rutgers University, Piscataway, New Jersey 08854, United States

ABSTRACT: A new empirical sampling method termed "temperature intervals with global exchange of replicas and reduced radii" (TIGER3) is presented and demonstrated to efficiently equilibrate entangled long-chain molecular systems such as amorphous polymers. The TIGER3 algorithm is a replica exchange method in which simulations are run in parallel over a range of temperature levels at and above a designated baseline temperature. The replicas sampled at temperature levels above the baseline are run through a series of cycles with each cycle containing four stages: heating, sampling, quenching, and temperature level reassignment. The method allows chain segments to pass through one another at elevated temperature levels during the sampling stage by reducing the van der Waals radii of the atoms, thus eliminating chain entanglement problems. Atomic radii are then returned to their regular values and re-equilibrated at elevated temperature prior to quenching to the baseline temperature. Following quenching, replicas are compared using a Metropolis Monte Carlo exchange process for the construction of an approximate Boltzmann-weighted ensemble of states and then reassigned to the elevated temperature levels for additional sampling. Further system equilibration is performed by periodic implementation of the previously developed TIGER2 algorithm between cycles of TIGER3, which applies thermal cycling without radii reduction. When coupled with a coarse-grained modeling approach, the combined TIGER2/TIGER3 algorithm yields fast equilibration of bulk-phase models of amorphous polymer, even for polymers with complex, highly branched structures. The developed method was tested by modeling the polyethylene melt. The calculated properties of chain conformation and chain segment packing agreed well with published data. The method was also applied to generate equilibrated structural models of three increasingly complex amorphous polymer systems: poly(methyl methacrylate), poly(butyl methacrylate), and DTB−succinate copolymer. Calculated glass transition temperature (T_g) and structural parameter profile ($S(q)$) for each resulting polymer model were found to be in close agreement with experimental T_g values and structural measurements obtained by X-ray diffraction, thus validating that the developed methods provide realistic models of amorphous polymer structure.

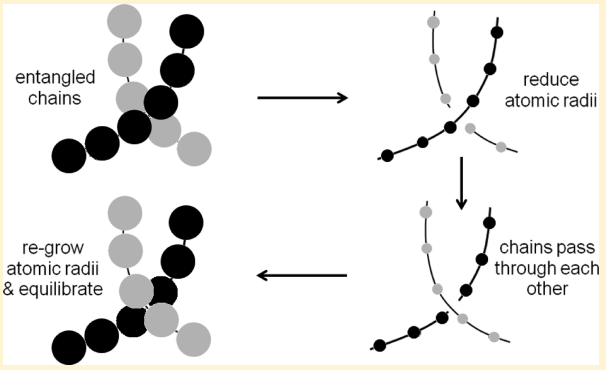

INTRODUCTION

Amorphous polymers are composed of densely packed, randomly entangled chains. The time scales associated with chain relaxations can range from picoseconds to microseconds or even longer even when the temperature is above the glass transition temperature (T_g) of the polymer, corresponding to the processes occurring over length scales ranging from the covalent bond length to the dynamical entanglement length of the polymer chains.[1,2] These factors make it extremely difficult to produce equilibrated molecular models of the amorphous phase of polymer structure. Recently, a number of efficient sampling techniques have been developed. For example, the method developed by Auhl et al.[3] is based on the prepacking of Gaussian chains and gradual introduction of the excluded volume. The pivot and bridging algorithms developed by Grest et al.[4] and Theodorou et al.[5] rapidly change the configuration of systems by forming new bonds across pairs of chains. These methods can be implemented for both lattice or off-lattice models and are applicable to both united and explicit atom simulations. The independence of overall relaxation time on chain length in these methods enables them to be applied in simulations of very long chains. However, there are still great demands in building unrestricted atomic models for investigating the effect of specific functional groups on system behavior or for the development of realistic all-atom structural models of a designated polymer with complex branching structures that can be used to study phenomenon such as water transport through the polymer or solute adsorption on the polymer's surface. However, given the fact that the longest

Received: January 25, 2011
Revised: May 4, 2011
Published: June 17, 2011

relaxation time of an entangled polymer network of chain length N scales as $N^{3.4}$ [2] and that CPU time scales as $N^{1.5}$,[5] leading to about N^5 in CPU time for adequate equilibration, the use of conventional molecular simulation methods to equilibrate amorphous polymers is prohibitively expensive. To meet this challenge, there is a distinct need to develop simulation methods that provide the ability to substantially reduce the number of degrees of freedom without losing atomic-level structure information on the system and to also solve the severe configurational sampling problem caused by chain entanglement so that realistic all-atom models of amorphous polymers can be efficiently constructed.

Recently, a number of computer modeling methods have been developed with the aim of efficiently equilibrating condensed-phase polymers with high chain-packing density. Among these methods, the coarse-graining technique is one of the most effective ways to accelerate the equilibration for dense systems.[6−11] This method provides a means of greatly reducing the number of degrees of freedom in the system while keeping the description of microscopic properties at the necessary level of accuracy and detail. To map an atomistic model onto a coarse-grained (CG) model, several atoms are grouped together into a relatively simple "superatom assembly" (or CG bead) and the interaction energies between respective CG beads are obtained by the application of an optimization procedure that reproduces the structural distributions obtained from atomistic simulations. With a CG model, the bulk structure of a polymer or polymer assemblies can be equilibrated in a much reduced time frame. The atomistic bulk structures can then be reconstructed from superpositions of atomistic counterparts on the corresponding CG beads. However, the coarse-graining method alone is not sufficient to solve the problem caused by chain-segment entanglement.

In the present work, we propose a new empirical sampling method to effectively overcome the entanglement problem and accelerate the equilibration of bulk-phase CG bead models of amorphous polymers. The method is based on the second version of a recently developed method named "temperature intervals with global exchange of replicas" (TIGER2),[12,13] which conducts a number of parallel molecular dynamics simulations at different temperature levels. In TIGER2, the replica at the baseline temperature goes through regular molecular dynamics while replicas at temperatures above the baseline go through a series of cycles with each cycle represented by a four-stage process of heating, sampling, quenching, and temperature level reassignment. The temperature level reassignment stage is conducted at the baseline temperature. At this stage, one of the quenched replicas is randomly selected and compared with the replica previously sampled at the baseline temperature using the Metropolis importance sampling criterion.[14] The unselected replicas then are reassigned to the higher temperature levels based on their potential energies. The new method proposed in this present paper is named "temperature intervals with global exchange of replicas and reduced radii" (TIGER3). TIGER3 is similar to TIGER2 in cycling. The difference between the two methods is that, in TIGER2, the defined van der Waals (VDW) radii of the force field values for the CG beads are used throughout the simulation; but in TIGER3, reduced VDW radii are used for the replicas that are heated and sampled at elevated temperatures, which enables chain segments to readily pass through one another. The reduced VDW radii method has been previously used by Curcó and Alemán as part of an energy minimization procedure in preparing the initial configurations for modeling dense polymer systems.[15] TIGER3, which is illustrated in Figure 1, incorporates this technique

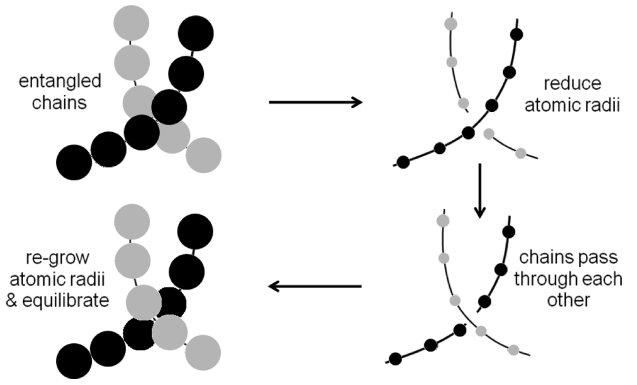

Figure 1. Schematic representation of the TIGER3 method.

into a replica exchange process with thermal energy being used to speed system equilibration. After a period of sampling, the VDW radii of the CG beads are recovered to their respective defined force field values; the recovered system is then energy minimized and equilibrated to eliminate overlaps among chain segments and then quenched down to the baseline temperature for replica comparison and temperature reassignment for the next sampling cycle. The temperature level reassignment stage after relaxation is similar to that used in TIGER2. By providing the ability for chains to pass through one another, followed by radii recovery and equilibration, the behavior of the polymer chains approximates that of ideal chains under theta-solvent conditions,[16] thus providing the means for the chains to organize in a manner that realistically represents dense-phase amorphous polymer structure.

The TIGER3 method provides the advantage of greatly accelerating the diffusion of chain segments in the dense system. It is noted that, similar to TIGER2, the new algorithm is also an empirical method and cannot be shown to rigorously satisfy the detailed balance condition. However, as addressed by Manousiouthakis and Deem,[17] detailed balance represents an overly strict condition that is sufficient but not necessary to provide a Boltzmann-weighted ensemble of sampled states, and the weaker balance condition requiring that the Markov process leaves the Boltzmann distribution invariant is necessary and sufficient for building Boltzmann-weighted ensembles of states. The ability of TIGER2 in establishing approximate Boltzmann-weighted ensembles has been empirically manifested by a number of simulations.[12,13] As demonstrated by this work, the combination of the TIGER2/TIGER3 algorithms provides an efficient approach for the equilibration of long-chain, entangled molecular systems and thus provides a useful method for the construction of realistic molecular models of dense-phase amorphous polymer structures.

METHODOLOGY

The examination of the TIGER3 method was first conducted by modeling a polyethylene (PE) melt and then using three sequentially more complex amorphous polymers: poly(methyl methacrylate) (PMMA), poly(butyl methacrylate) (PBMA), and DTB−succinate copolymer (DTBS). PE was chosen because it represents the simplest, very well characterized polymer with well documented conformational and structure packing information.[18−20] PMMA, PBMA, and DTBS were selected to provide much more complex amorphous polymer structures with increasing size of side chain. The glass transition temperatures

(T_g) for PMMA and PBMA are available from published sources,[21,22] while the T_g for DTBS was determined by differential scanning calorimetry (DSC). X-ray diffraction experiments were conducted to measure the scattering structure factors of the three amorphous polymers so that the accuracy of the simulation method could be evaluated by comparing the simulation results to those obtained experimentally. This section introduces the methods used in the present work, including the approach used to develop CG parameters for the polymers, the details of the TIGER3 algorithm, the setup of the simulations that were conducted to produce structural models of each polymer, and the experimental methods used for measuring T_g and $S(q)$.

Coarse-Graining Models of Polymers. The coarse-graining force field was developed using the CHARMM molecular simulation package,[23,24] internally adapted by our group to use the polymer consistent force field (PCFF),[25−28] in which the all-atom model total force field energy (E) is calculated by

$$E = E_{\text{bonded}} + E_{\text{nonbonded}} \tag{1}$$

where E_{bonded} and $E_{\text{nonbonded}}$ are bonded and nonbonded potential terms, respectively. These terms are decomposed as

$$\begin{aligned} E_{\text{bonded}} &= E_{\text{stretch}} + E_{\text{bend}} + E_{\text{torsion}} + E_{\text{cross}} \\ E_{\text{nonbonded}} &= E_{\text{VDW}} + E_{\text{Coulomb}} \end{aligned} \tag{2}$$

where E_{stretch}, E_{bend}, and E_{torsion} are the bond-length-stretching, angle-bending, and bond-rotation energies, respectively; the cross-term, E_{cross}, accounts for the coupling between individual bonded interactions; E_{VDW} accounts for the excluded volume repulsive as well as the intermolecular attractive forces between nonbonded atoms; and E_{Coulomb} is the electrostatic potential. The CG force field was developed in a similar manner with a few modifications. Specifically, the E_{cross} term was not considered, and the electrostatic interactions between nonbonded superatoms were reasonably ignored since all CG beads were constructed to be net-neutral. Therefore, the potential terms that need to be parametrized included E_{stretch}, E_{bend}, E_{torsion}, and E_{VDW}. For each term, CG parametrization was conducted based on the iterative Boltzmann inversion of the corresponding atomistic distribution functions.[10,11] During the iterative procedure for a particular distribution, the rest of the potentials were kept constant. In dense systems, individual distributions usually depend on the full set of potentials through higher-order correlations, requiring that individual potentials must be readjusted after other interactions are changed. In practice, the iteration is usually started with the potentials that are least affected by changes of others. According to the suggestion of Reith et al.,[10] the potential terms were therefore optimized in the order of their relative strength, with parametrization systematically developed in the order of $E_{\text{stretch}} \rightarrow E_{\text{bend}} \rightarrow E_{\text{VDW}} \rightarrow E_{\text{torsion}}$.

The Boltzmann-inversion method performs potential inversion from a set of known distributions of structural parameters (e.g., from the atomistic simulation) to extract effective CG potentials. The potentials calculated from the Boltzmann-inversion methods must reproduce the distributions of structural parameters for various bonds, bond angles, dihedral angles, and intermolecular radial distribution functions extracted from reference atomistic simulations. Following our previous work,[29] the distributions of bond lengths and bond angles were fitted by a double Gaussian function and the distributions of dihedral angles were fitted by 3-fold Fourier progression forms. The parametrization of the VDW interactions was conducted for compounds that have similar atomic structures to the superatoms in the CG model. The details of the approaches to calculate the four types of potentials are provided in ref 29.

Mixed Sampling Scheme with TIGER3 and TIGER2. In the actual use of the TIGER3 algorithm, we found that if the VDW radii of the CG beads were reduced in every cycle, the relaxation of high energy states caused by overlaps among chain segments when radii were returned to their normal values became increasingly more inefficient as the simulation continued. This led to high energy states in the quenched replicas and thus an unacceptably low exchange acceptance ratio between the baseline and the quenched replicas. An effective way to solve this problem was found by using a mixed scheme of TIGER2 and TIGER3, in which TIGER3 cycling was carried out periodically to rapidly change the configurations of the system by allowing the crossover of chain segments, with the TIGER2 algorithm then periodically being applied to relax the system recovered from the series of TIGER3 cycles. The ratio of TIGER2 to TIGER3 cycles implemented in the mixed method was determined by the value of the exchange acceptance ratio that was obtained from a pretest run. Typically, we found that a pretest run with PMMA using one TIGER3 cycle for every ten TIGER2 cycles provided about 35% exchange acceptance ratio, and thus a 1: 10 ratio of TIGER3 to TIGER2 cycles was selected in all subsequent simulations.

While the details regarding how to perform a TIGER2 simulation have been previously published,[12,13] they are briefly summarized here. A TIGER2 process is composed of a number of replicas of the molecular system (N_r). The replica at baseline temperature (T_B) undergoes sampling via regular molecular dynamics while the rest of replicas are conducted through a series of sampling cycles with each cycle containing four stages: (1) rapid heating from T_B to the designated elevated temperature (T_m) by rescaling the momenta of the atoms within the replica by a factor of $(T_m/T_B)^{1/2}$ and thermally equilibrating, (2) molecular dynamics sampling at the constant elevated temperature level (T_m), (3) rapid quenching back down to T_B by rescaling the momenta by a factor of $(T_B/T_m)^{1/2}$ followed by thermal equilibration, and (4) global replica reassignment. Stage 4 consists of two substeps: (i) One state from among the set of $(N_r - 1)$ quenched states is randomly selected, and the potential energy of this state is then compared with the state from the production run of the baseline replica using the Metropolis importance sampling criterion[14]

$$\min\{1, \exp[-(E_i - E_B)/k_B T_B]\} \tag{3}$$

where E_i is the potential energy of the selected quenched state and E_B is the potential energy of the baseline state, and the exponential expression is the probability that the quenched state "i" will be exchanged for the baseline state B. (ii) All replicas except the selected baseline replica are then reassigned to the higher temperature levels according to their potential energies; i.e., a higher potential energy state is assigned to a higher temperature level. It is noted that in TIGER2 the VDW interaction parameters adopt their regular force field values throughout the simulation. The strategy of how to determine the length of each stage in a TIGER2 cycle has been studied in ref 13, which determined that the proper lengths for heating, sampling, and quenching are about 1−2, 4−6, and 2−4 ps, respectively.

A TIGER3 process is similar to that of TIGER2 in many aspects. However, in TIGER3, the sampling stage at elevated temperature levels is conducted with four substeps under constant

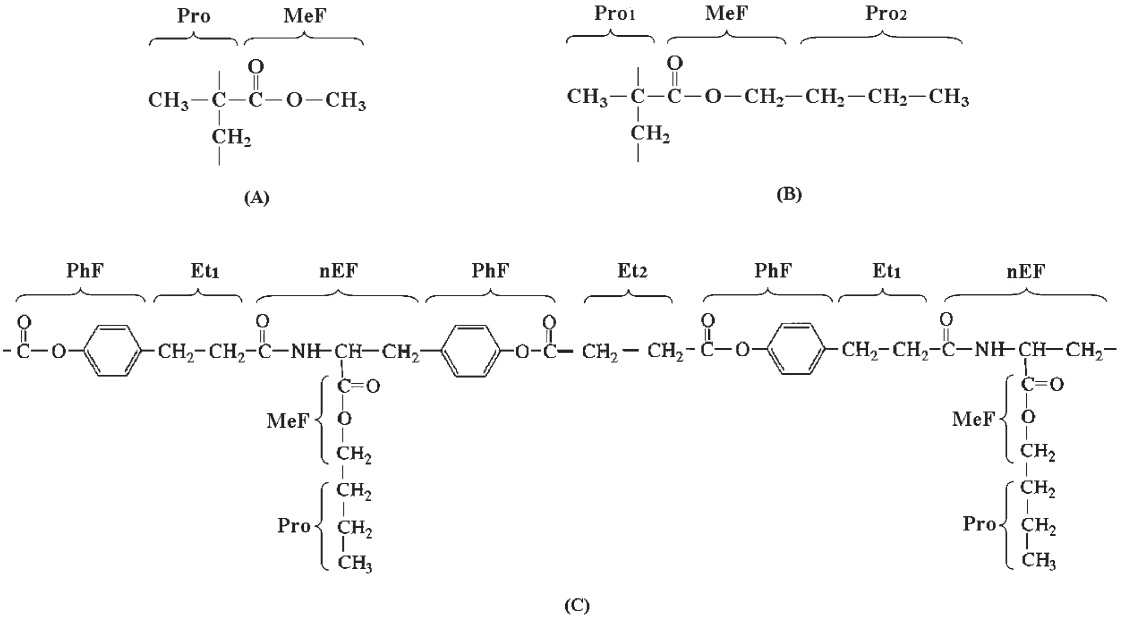

Figure 2. Schematic representations of the atomic and the CG models for (A) PMMA, (B) PBMA, and (C) DTBS. Abbreviations for CG bead segments: propane (Pro), methyl formate (MeF), phenyl formate (PhF), ethane (Eth), *n*-ethylformamide (nEF).

volume conditions composed of (1) Monte Carlo (MC) sampling with reduced VDW radii (we used zero VDW radii to turn off both attraction and repulsion terms), (2) energy minimization with the VDW radii recovered to their regular force field values, (3) relaxation using the MC method, and (4) molecular dynamics sampling for further equilibration. In most of the cases (i.e., >90%), the overlaps resulting from substep 1 can be eliminated after substep 3, but in the situation where the overlaps cannot be effectively eliminated, thus leading to extremely high potential energy that exceeds the upper limit of a real-type variable defined in CHARMM,[23,24] the new configuration is rejected and the structure that resulted following the heating stage of the TIGER3 cycle is used to restart the molecular dynamics sampling at substep 4. In that case, the sampling provided using the TIGER3 algorithm is no different than the TIGER2 algorithm.

Molecular Models and Setup of Simulations. Five different molecular models were considered: a single chain of polyethylene (PE), a PE melt, and amorphous chains of PMMA, PBMA, and DTBS (Figure 2). All simulations were carried out with the CHARMM program[23,24] using the Nose-Hoover thermostat[30−32] for constant volume and constant temperature. For atomic model calculations, the SHAKE algorithm[23] was used to constrain all bond lengths containing hydrogen. The velocity-Verlet algorithm[23,33] was used with a time step of 1 fs to integrate the equations of motion in the dynamics simulations. All simulations were performed with an atom-based 14 Å cutoff.

In all TIGER2/TIGER3 simulations, one TIGER3 cycle was applied after ten TIGER2 cycles, which we refer to as a 10:1 TIGER2/TIGER3 scheme. A pretest based on the PMMA system (using eight replicas with temperature levels ranging from 295 to 620 K) indicated that the 10:1 scheme provides an exchange acceptance ratio of greater than 35%. The TIGER2 cycle involved a sequence of 2 ps heating, 4 ps sampling, and 4 ps quenching and relaxation processes. The TIGER3 cycle includes similar heating and quenching processes as those in TIGER2, but with the implementation of the above-described substeps at each elevated temperature, which were composed of (1) 10^6 steps of MC sampling for the dihedral angles conducted with zero VDW radii, (2) energy minimization with recovered VDW radii conducted with 500 steps of steepest descent (SD) method followed by another 500 steps of adopted basis Newton−Raphson (ABNR) method,[23] (3) 10^6 steps of MC sampling for the dihedral angles and atom positions, and (4) 4 ps molecular dynamics sampling. To be consistent to our previous work,[13] all TIGER2/TIGER3 simulations used eight replicas at evenly spaced temperature levels. The temperature difference between successive levels is typically set to be between 40 and 50 K.

TIGER2/TIGER3 Tests on Polyethylene. A set of single PE chains in vacuum with chain lengths of $N = 64$, 128, 256, and 512 mer units (denoted as C_{64}, C_{128}, C_{256}, and C_{512}) were sampled in the TIGER2/TIGER3 simulations. For the C_{64} system, a conventional replica-exchange molecular dynamics (REMD) simulation[34] was conducted. Then the corresponding results of distributions of torsional angles and potential energy density from the two simulation methods were compared. Further tests on the TIGER2/TIGER3 method were conducted by modeling a dense system of PE melt composed of 21 PE chains with each chain containing 96 mer units (denoted as C_{96}). In these simulations, a PE chain was represented by a CG model in which the $-CH_3$ and $-CH_2-$ groups were represented by simple spherical beads. For simplicity, we used the parameters of the united atom model of butane given by the CHARMM force field (PARAM19) for the CG bead segments. Starting from an extended conformation of the PE chain, 30 ns simulations were conducted for the single chain tests. The TIGER2/TIGER3 simulations used eight replicas at evenly spaced temperature levels ranging from 400 to 680 K, while the REMD simulations used 24 replicas at exponentially spaced temperature levels (as recommended for REMD) over this same temperature range. In the REMD simulations, the attempts of swapping between adjacent replicas were made every 1 ps. The baseline temperature

Table 1. Summary of the Atom Connections in the CG Model of PMMA and PBMA

	bond		bond angle		dihedral angle	
type of polymer	connection	label	connection	label	connection	label
PMMA	Pro−Pro	l_1	Pro−Pro−Pro	θ_1	Pro−Pro−Pro−Pro	φ_1
	Pro−MeF	l_2	Pro−Pro−MeF	θ_2	Pro−Pro−Pro−MeF	φ_2
					MeF−Pro−Pro−MeF	φ_3
PBMA	Pro_1−Pro_1	l_1	Pro_1−Pro_1−Pro_1	θ_1	Pro_1−Pro_1−Pro_1−Pro_1	φ_1
	Pro_1−MeF	l_2	Pro_1−Pro_1−MeF	θ_2	Pro_1−Pro_1−Pro_1−MeF	φ_2
	Pro_2−MeF	l_3	Pro_1−MeF−Pro_2	θ_3	MeF−Pro_1−Pro_1−MeF	φ_3
					Pro_1−Pro_1−MeF−Pro_2	φ_4

(400 K) was selected to be close to the melting point of PE (410 K). In the TIGER/TIGER2 simulation for C_{96} PE melt, the initial conformation was prepared by collapsing a single chain of PE containing 2016 mer units into a cubic box with a dimension of $39.1 \times 39.1 \times 39.1$ Å^3 and then breaking the long chain into 21 short C_{96} chains. The new system was then energy minimized and relaxed with molecular dynamics for 100 ps with periodic boundary conditions imposed. Starting from the resulted structure, a 30 ns TIGER2/TIGER3 simulation was conducted with eight replicas at evenly spaced temperature levels ranging from 400 to 680 K. From the simulation, the properties of chain conformation, chain segment positional order, and orientational order were determined. The conformation of the PE chains at equilibrium was characterized by the mean-square radius of gyration $\langle R_G^2 \rangle$, the end-to-end distance, $\langle R^2 \rangle$, and the characteristic ratio $\langle R^2 \rangle/(N-1)l^2$, where $N-1$ is the number of bonds and l is the bond length.

The positional order of chain segments provides information on chain segment packing in the bulk. It is characterized by the intermolecular pair distribution function, which measures the probability to find a pair of intermolecular sites and is calculated by

$$g(r) = \frac{\langle n(r) \rangle}{4\pi r^2 dr \rho} \tag{4}$$

where $\langle n(r) \rangle$ is the average number of intermolecular atom pairs at distance r and ρ is the bulk number density. Experimentally, the positional order of chain segments in bulk is observed by measuring the X-ray structure factor, $S(q)$, which can be theoretically calculated based on the Fourier transform of the total pair distribution function[35]

$$S(q) = 1 + 4\pi\rho \int_0^\infty r \frac{\sin(rq)}{q} [G^t(r) - 1] \, dr \tag{5}$$

where q is the magnitude of the scattering vector and $G^t(r)$ is the total pair distribution function including the contributions of both intra- and interchain atom pairs.

The orientational order between intermolecular bonds is useful information in understanding chain packing. It is characterized by the intermolecular orientational correlation function collected for vectors bisecting two successive bond segments[18] and is calculated by

$$s(r) = \frac{1}{2}\left[3\langle \cos^2 \theta(r) \rangle - 1\right] \tag{6}$$

where θ is the angle between a pair of bisecting vectors at distance r. In practice, the weighted intermolecular orientational correlation function, $s(r)g_v(r)$, is considered, in which $g_v(r)$ is the intermolecular two-bond segment (or the bisecting vector) pair distribution function.

Coarse-Grained Model Parameterization for PMMA, PBMA, and DTBS. The details of the CG parameter development procedures are presented here only for PMMA and PBMA, with parameters for DTBS being obtained from a previous publication.[29] The chemical repeat units of each of these polymers along with their designated superatom groupings are shown in Figure 2. A 2:1 mapping scheme was used for PMMA (Figure 2A), in which each repeat unit was represented by two spherical beads, corresponding to (1) a propane (Pro) subunit containing the main-chain atoms and the α-methyl group and (2) a methyl formate (MeF) subunit containing the ester side group. PBMA was coarse-grained with a 3:1 mapping scheme, in which each repeat unit was represented by three CG beads (Figure 2B), corresponding to (1) a Pro1 subunit, (2) a MeF subunit, and (3) a Pro2 subunit. Subunit 1 forms the main chain, while subunits 2 and 3 form the side chain. As shown in Figure 2C, DTBS represents a much more complex structure with the mer structure being represented by six different types of CG beads.[29] For all CG models, the mapping point is taken as the center of mass of each bead. The presence of different types of CG beads in these polymers introduces new CG potentials. The compositions of the new CG bonds, bond angles, and dihedral angles are summarized in Table 1 for PMMA and PBMA, and readers are referred to ref 29 for the CG parameters for DTBS. These parameters were developed to optimally represent the behavior of all-atom models of these same polymer systems following the methods that are described in detail in ref 29, which are summarized in the following paragraph.

The CG parameters for PMMA and PBMA were obtained by first conducting atomistic simulations with the PCFF force field using the TIGER2 sampling method for single PMMA and PBMA hexamers (containing six repeat units) in order to get the target distributions of bond length, bond angle, and dihedral angle that were subsequently used to derive CG-bead model parameters for each polymer. On the basis of the work of Lovell and Windle,[36] which indicated that typical amorphous PMMA is largely composed of syndiotactic mer units, we used a fully syndiotactic conformation in the initial atomic structure of PMMA. However, for PBMA with its longer side chain, the atactic conformation in the initial atomic structures was used. Starting from an extended conformation, each polymer hexamer was equilibrated with the TIGER2 method using eight replicas at evenly spaced temperature levels ranging from 500 to 780 K. The 500 K baseline temperature was selected based on the value used in the work of Chen et al.[37] and is higher than the glass transition

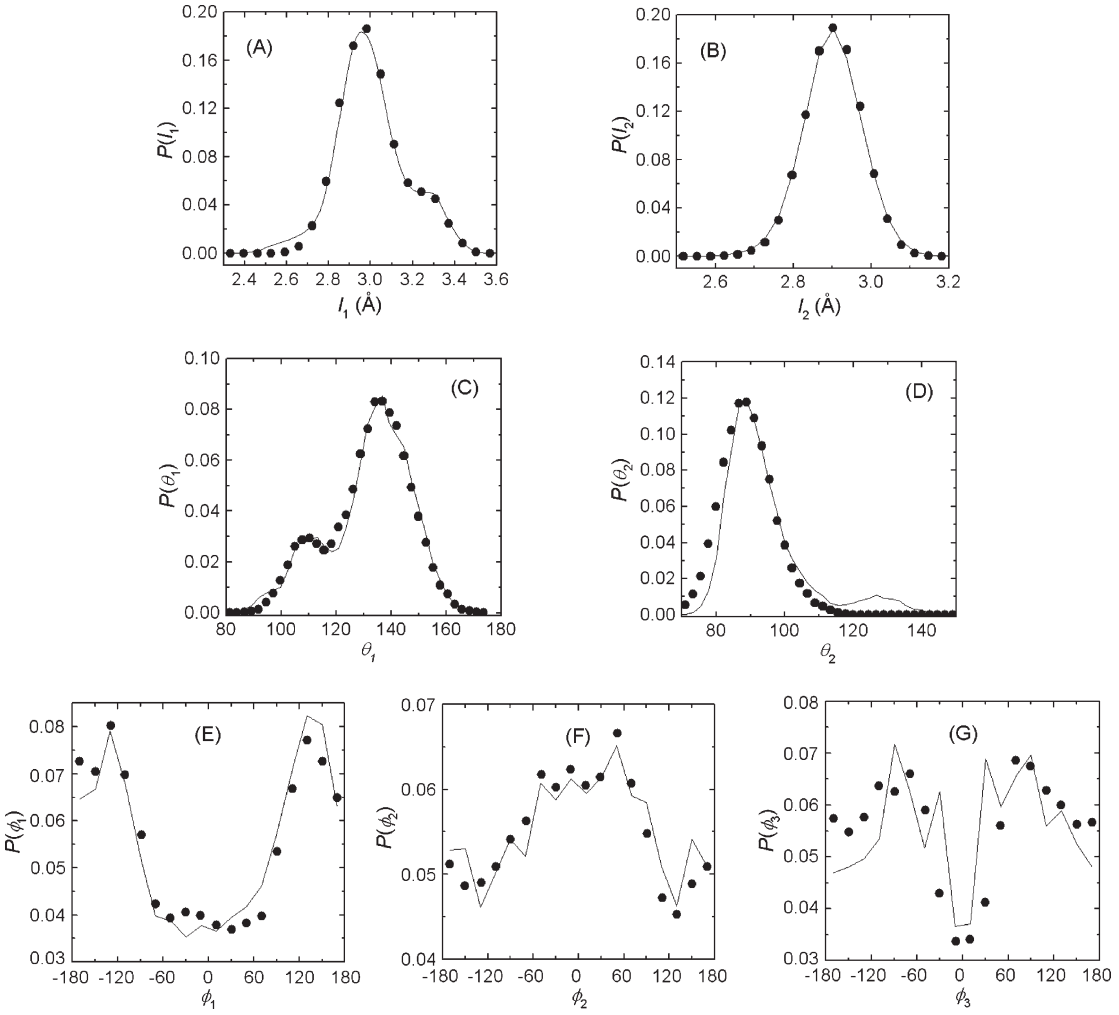

Figure 3. Parameter development for PMMA. Distributions comparing behavior of atomistic models (dots) and CG bead models (lines) for bond lengths for l_1 (A) and l_2 (B); bond angles θ_1 (C) and θ_2 (D); and dihedral angles φ_1 (E), φ_2 (F), and φ_3 (G). Bond types are defined in Table 1.

Table 2. Bond Stretching Interaction Parameters for the CG Model of PMMA and PBMA Fitted by the Double Gaussian Function [Eq 4 in Ref 29] for the Atomistic Distributions

polymer	bond	l_{c1} (Å)	l_{c2} (Å)	K_{b1} (Å^{-2})	K_{b2} (Å^{-2})	K_{b3}
PMMA	Pro−Pro	2.853	2.887	93.518	74.017	0.265
	Pro−MeF	2.439	2.472	95.296	85.650	1.076
PBMA	Pro_1−Pro_1	2.942	3.273	24.601	64.259	0.358
	Pro_1−MeF	2.844	2.878	53.515	98.478	1.683
	Pro_2−MeF	3.500	3.881	8.823	10.314	2.190

Table 3. Bending Interaction Parameters for the CG Model of PMMA and PBMA Fitted by the Double Gaussian Function [Eq 6 in Ref 29] for the Atomistic Distributions

polymer	angle	θc_1 (deg)	θc_2 (deg)	$K_{\theta 1}$ (rad^{-2})	$K_{\theta 2}$ (rad^{-2})	$K_{\theta 3}$
PMMA	Pro−Pro−Pro	124.463	153.642	31.526	73.154	2.562
	Pro−Pro−MeF	89.461	106.867	20.072	6.358	1.142
PBMA	Pro_1−Pro_1−Pro_1	118.014	146.603	11.591	15.526	0.703
	Pro_1−Pro_1−MeF	90.806	110.838	17.954	6.197	0.480
	Pro_1−MeF−Pro_2	113.958	134.433	25.510	7.504	1.516

temperatures of both PMMA and PBMA. For each hexamer, the molecular structure obtained from the 500 K replica following 20 ns of TIGER2 cycling was saved and then mapped onto a CG structure. After the CG parameters were obtained, TIGER2 simulations using a similar protocol were conducted with the CG models of PMMA and PBMA hexamers to further refine the CG parameters until the structure distributions calculated from the CG model optimally matched the corresponding results calculated from the atomistic model.

Bulk-Phase Models of PMMA, PBMA, and DTBS. Once the parameters of the CG models of the three polymers were optimized for agreement with their respective all-atom models, the CG models were then used in the TIGER2/TIGER3 simulations to relax the bulk-phase models of each polymer. The model systems of PMMA and PBMA consisted of 32 chains, while the DTBS system with its much larger mer structure contained 16 chains. In all systems, each chain contained 16 repeat units. To prepare the starting configuration of each system, molecular dynamics calculations were performed at 500 K to relax the chains, which were initially structured in their fully extended conformations. A 0.1 kcal/mol harmonic potential was imposed

dx.doi.org/10.1021/ma200128c |*Macromolecules* 2011, 44, 5452–5464

Table 4. Optimized CG Parameters for Dihedral Interaction Term for PMMA and PBMA Fitted by the Torsional Potential [Eq 8 in Ref 29] for the Atomistic Distributions

polymer	angle	K_1 (kcal/mol)	K_2 (kcal/mol)	K_3 (kcal/mol)	$\delta_{i=1,3}$
PMMA	Pro−Pro−Pro−Pro	−1.620	−0.050	0.050	0
	Pro−Pro−Pro−MeF	0.010	0.010	−0.050	0
	MeF−Pro−Pro−MeF	0.020	−0.020	−0.010	$\pi/3$, 0, 0
PBMA	Pro_1−Pro_1−Pro_1−Pro_1	−0.260	−0.040	0.100	0
	Pro_1−Pro_1−Pro_1−MeF	0.120	0.010	0.110	$\pi/3$
	MeF−Pro_1−Pro_1−MeF	−0.030	−0.040	0.180	0
	Pro_1−Pro_1−MeF− Pro_2	0.310	−0.440	0.040	π, $\pi/3$, 0

on beads beyond a defined distance away from the central point to compress and then constrain all chain segments within a sphere with radius of 20.5 Å for PMMA, 24 Å for PBMA, and 27.5 Å for DTBS. The harmonic constraint was then removed, and the periodic boundary condition was imposed with dimensions 41.50 × 41.50 × 41.50 $Å^3$ for PMMA, 48.65 × 48.65 × 48.65 $Å^3$ for PBMA, and 55.50 × 55.50 × 55.50 $Å^3$ for DTBS, respectively, such that the initial spherical model of each polymer system fit within the defined periodic boundary, with the polymer then expanding out to uniformly fill the defined boundary space within the first 1.0 ns of simulation. These dimensions were set to provide system densities of about 1.19, 1.05, and 1.20 g/cm^3 when the periodic box were completely filled, which were matched to the bulk densities for these respective polymers in their amorphous state. The structures in the periodic box were then relaxed for 140 ns with the TIGER2/TIGER3 method using eight replicas with temperature levels being evenly distributed between 295 and 620 K. Each relaxed structure was then used as input for the calculation of T_g. For PMMA, an independent 140 ns TIGER2 simulation alone was conducted with eight replicas in order to compare the performance of TIGER2 by itself with the combined TIGER2/TIGER3 method.

The T_g for PMMA, PBMA, and DTBS were calculated based on the equilibrated bulk-phase model represented by the CG models. Conventional molecular dynamics calculations were carried out at 12 temperatures ranging evenly spaced from 250 to 550 K for PMMA, from 150 to 450 K for PBMA, and from 200 to 550 K for DTBS, respectively. For each case, three 600 ps trajectories were generated. Followed the analysis by Tsige and Taylor,[38] T_g can be estimated by examining the influence of temperature on the mean-square displacement (MSD) of atoms in the system. In a dynamics process, the mean-square displacement, g_0, of an atom from its initial position is defined as

$$g_0(t) = \langle [\mathbf{r}(t) - \mathbf{r}(0)]^2 \rangle \quad (7)$$

where $\mathbf{r}(0)$ and $\mathbf{r}(t)$ are positions of an atom at time 0 and t, and $\langle \cdots \rangle$ denotes the average over all atoms and all times t. MSD measures the overall dynamics of a polymer system and can be directly extracted from the trajectory of a molecular dynamics simulation.

After obtaining the equilibrated bulk-phase CG structures for each polymer, we selected the lowest energy state from the last 20 ns CG structures and conducted reverse mapping based on the methods presented in ref 29 to obtain the atomistic bulk-phase model for each polymer. The recovered structures were energy minimized and equilibrated with the TIGER2 method for 1 ns. These relaxed structures were used as the inputs for the conventional MD calculations. The last 10 ps MD trajectory was then used to estimate of $S(q)$ for each polymer for comparison with the experimental results, which were obtained by X-ray diffraction. The profile of $S(q)$ was calculated by eq 5

Experimental Measurement of T_g and $S(q)$ for Polymer Model Validation. The T_g for PMMA and PBMA are well-known and were obtained from published sources,[21,22] while the T_g for DTBS was determined using 10 mg of sample on a TA Instruments DSC 2920 calibrated with an indium standard. Measurements were made under a nitrogen atmosphere at 10 °C/min. The T_g was evaluated from the second heating scan as the temperature at half of total specific heat change between extrapolated tangents at the beginning and the end of the transition.

To measure the $S(q)$ for the three polymers, X-ray experiments were performed on beamline 11 ID-C at the Advanced Photon Source (APS) at Argonne National Laboratory, Argonne, IL. Samples for X-ray scattering were inserted into 2 mm diameter X-ray quartz capillaries, and data were collected in transmission geometry at ambient temperature. A 115 keV X-ray beam (wavelength λ = 0.1078 Å) from a Si(311) Laue monochromator that was collimated to a size of about 0.2 × 0.2 mm was used. Diffraction patterns were collected using a Perkin-Elmer amorphous silicon 1621 AN3 detector with a sample-to-detector distance of 661 mm. Data from a q of 0.5−20 $Å^{-1}$ was used in the analysis; q is the scattering vector and is defined as $q = [(4\pi \sin\theta)/\lambda]$, where 2θ is the scattering angle. X-ray scattering data were obtained for a total of 800 s in five sequences, each sequence consisting of 20 frames, with 8 s exposure per frame exposures. The background was measured using an empty 2.0 mm quartz capillary. The raw data were integrated and converted to intensity versus q, using the Fit2D software.[39] The observable in the scattering experiment is the coherent X-ray scattering intensity, $I_{coh}(q)$, from which the total structure function $S(q)$ is derived using the expression

$$S(q) = \frac{I_{coh}(q) - \sum_i x_i f_i^2(q)}{\left[\sum_i x_i f_i^2(q)\right]^2} \quad (8)$$

where for atomic species i, x_i and f_i are the atomic fraction and X-ray form factor, respectively. $S(q)$, with corrections for sample absorption, Compton scattering, and multiple scattering, was calculated using the PDFgetX2 program.[40] Because of the high energy of the X-rays and the transmission geometry used for these measurements, the corrections for sample absorption and multiple scattering are negligible.

RESULTS AND DISCUSSION

Coarse-Grained Model Parameters for PMMA, PBMA, and DTBS. The CG parameters of the DTB succinate model have

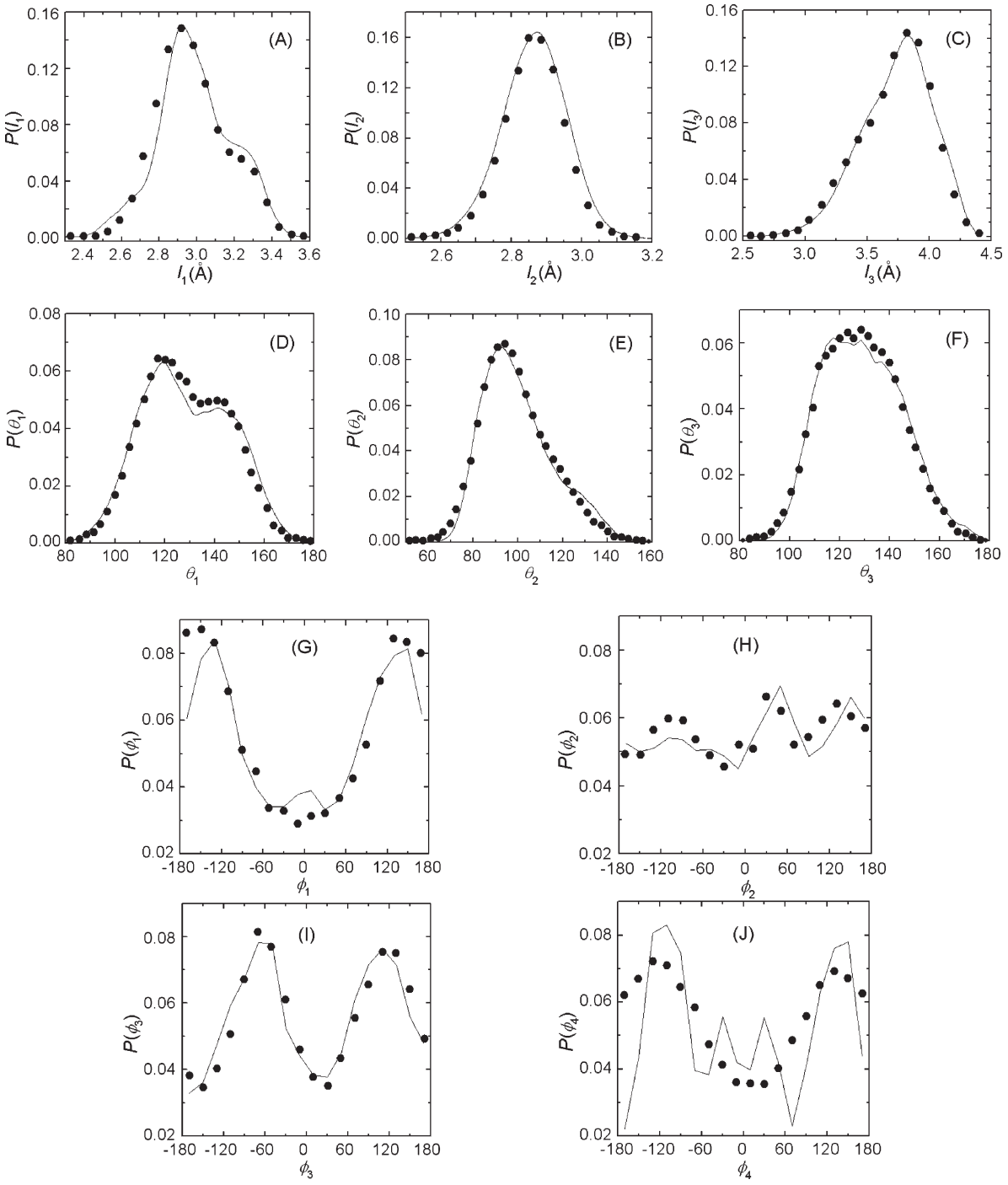

Figure 4. Parameter development for PBMA. Distributions comparing behavior of atomistic models (dots) and CG bead models (lines) for bond lengths for l_1 (A), l_2 (B), and l_3 (C); bond angles θ_1 (D), θ_2 (E), and θ_3 (F); and dihedral angles φ_1 (G), φ_2 (H), φ_3 (I), and φ_4 (J). Bond types are defined in Table 1.

been developed in our previous work and are presented in ref 29. In the present work, the TIGER2 method was applied to initially sample the atomistic models of the PMMA and PBMA hexamers. Based on the 20 ns trajectories of the atomistic simulations, the distributions of structural factors were determined, from which the bonded parameters of the CG force field were derived. For PMMA, the distributions of distances between adjacent superatoms and the distributions of bond angles between three successive superatoms obtained from atomistic calculation (scattered dots) are shown in parts A, B and C, D of Figure 3, respectively. These profiles were fitted with the double Gaussian functions given by eqs 4 and 6 in ref 29. The fitted parameters for bond-length stretching interactions and bond-angle bending interactions are given in Tables 2 and 3, respectively. The calculation results of the target distributions of the three types of dihedral angles given in Table 1 are shown in Figure 3E−G with scattered dots. The force constants, K_i, and phase angles, δ_i ($i = 1, 3$), were optimized so that, based on the torsional potential

dx.doi.org/10.1021/ma200128c |*Macromolecules* 2011, 44, 5452–5464

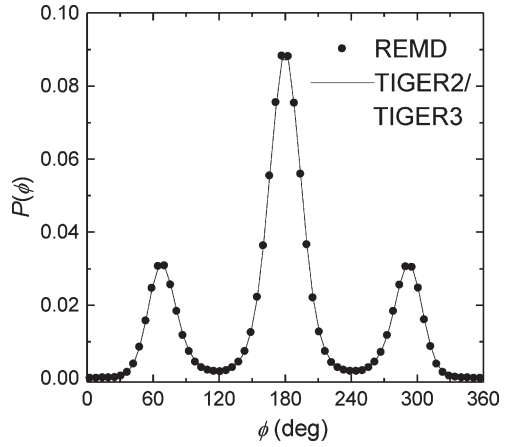

Figure 5. Comparison of the torsional angle distributions calculated based on REMD (circles) and TIGER2/TIGER2 (line) methods for single C_{64} PE chain.

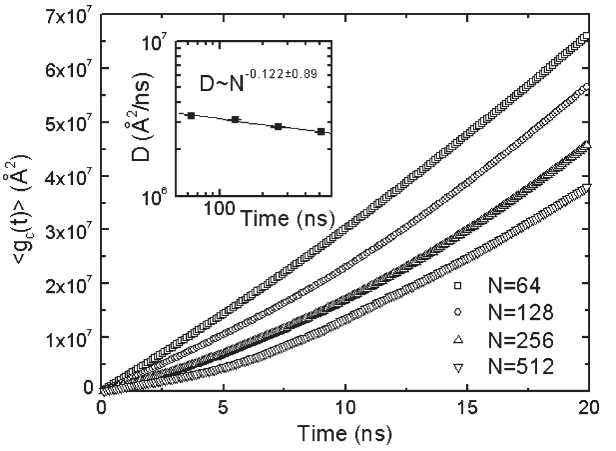

Figure 7. Mean-square displacement of center of mass from TIGER2/TIGER3 simulations for PE. Inset: dependence of the self-diffusion coefficient on chain length.

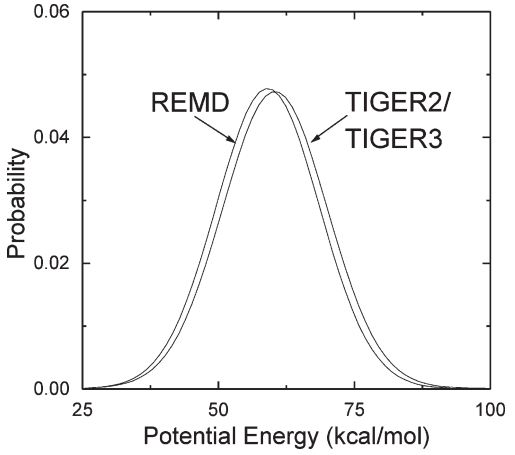

Figure 6. Comparison of the potential energy distributions calculated based on REMD and TIGER2/TIGER2 methods for single C_{64} PE chain.

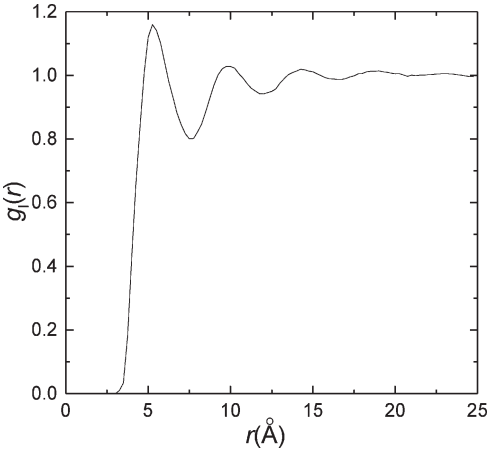

Figure 8. Intermolecular pair distribution function for C_{96} PE melt at 400 K from a TIGER2/TIGER3 simulation.

defined by eq 8 in ref 29, the distributions of dihedral angle calculated by the CG model could optimally reproduce the target distributions. The optimized parameters are given in Table 4. For the two types of beads (Pro and MeF) in the CG models of both PMMA and PBMA, the VDW parameters were obtained by mapping the radial distribution function of all-atom models of monodispersed compounds in their liquid state that have similar chemical structure as the superatoms in the polymer. These parameters had been calculated in our previous work (Table 5 in ref 29). A TIGER2 simulation was then conducted based on the above CG parameters of PMMA, and the CG parameters were further optimized so that the structural distributions obtained with the CG model matched the corresponding distributions obtained with the atomic model of PMMA. The converged CG distributions are plotted in Figure 3A−G with solid lines. The CG parameters for PBMA model were developed in a similar way, and the converged parameters are given in Tables 2, 3, and 4 for bond-length stretching, bond-angle bending, and dihedral-angle interactions, respectively. The corresponding results calculated with atomic and CG models are shown in Figure 4A−J.

Performance of the TIGER2/TIGER3 Method. The performance of the new TIGER2/TIGER3 scheme was evaluated for both accuracy and efficiency in sampling the model molecular systems by comparisons with sampling provided by REMD and TIGER2 simulations. Furthermore, the ability of TIGER2/TIGER3 simulations to generate realistic representative structures of bulk-phase amorphous polymers was assessed by comparing calculated values of T_g and $S(q)$ from the final equilibrated polymer models with experimentally measured values.

TIGER2/TIGER3 Tests on Polyethylene. The calculated distributions of torsional angles from the 30 ns TIGER2/TIGER3 and REMD simulations based on the united atom model of a C_{64} PE chain are plotted in Figure 5, which presents that the distributions obtained from the TIGER2/TIGER3 simulation are consistent with the corresponding results obtained from the REMD simulation. The ratio of the probabilities of the conformer in a trans vs a gauche state is about 2:1 and is consistent to the theoretical value of 2:1 calculated using the 0.7 kcal/mol energy barrier between the gauche and trans conformers,[23,41] Figure 6 compares the probability profiles of potential energy obtained from the REMD and TIGER2/TIGER3 simulations

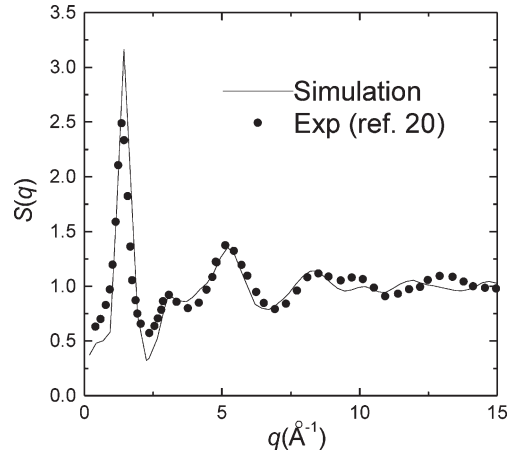

Figure 9. Structure factor, S(q), obtained from experiment (circles) for C_{6400} PE at 430 K_{20} and TIGER2/TIGER3 simulation (line) for C_{96} PE melt at 400 K.

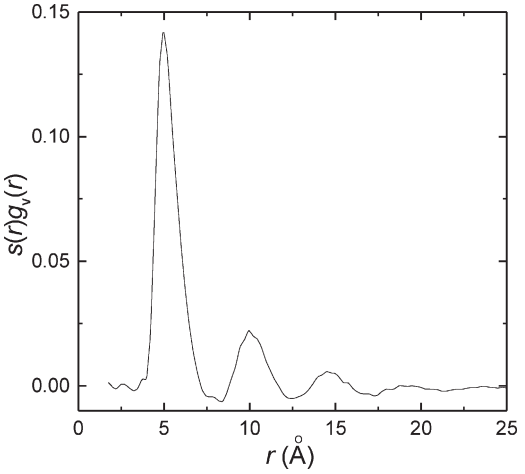

Figure 10. Weighted intermolecular orientational correlation function for two-bond segments in C_{96} PE melt at 400 K from a TIGER2/TIGER3 simulation.

for C_{64}. The average potential energies are 59.1 ± 9.5 and 60.4 ± 9.7 kcal/mol for REMD and TIGER2/TIGER3 simulations, respectively. The p-values for the Student's t test and F-test conducted based on the 5% significance level are 6% and 28%, respectively, indicating that both the means and the variance of the two energy distributions are not significantly different and that TIGER2/TIGER3 sampling is able to generate an ensemble of states that closely approximates a Boltzmann distribution.

The mobility of the polymer chain in a TIGER2/TIGER3 simulation determines the efficiency of the algorithm in relaxing the polymer structure. To estimate the chain mobility, we calculated the self-diffusion coefficient, D, of single PE chain of different chain lengths, N. For each single chain system, D was directly estimated from the slope of the linear regime of mean-square displacement profile of the center of mass of the polymer coil (Figure 7). The dependence of D on N is presented in the double-logarithmic scale as the inset of Figure 7, where $D \sim N^{-0.122\pm0.089}$ is obtained. The scaling of the diffusion coefficient is much smaller than the Rouse (N^{-1}) scaling,[2] indicating that

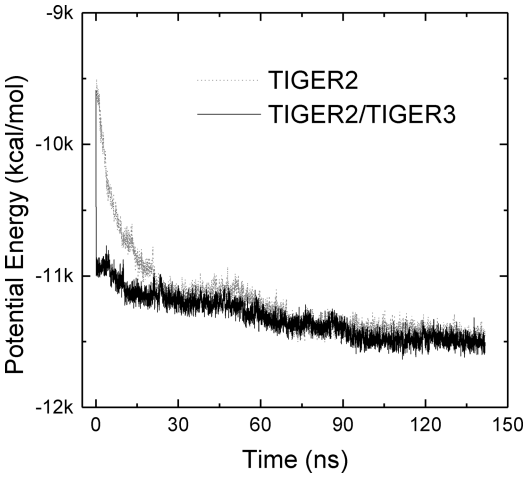

Figure 11. Temporal evolution of the potential energy obtained from PMMA simulations with TIGER2 (dotted line) and TIGER2/TIGER3 (straight line) schemes.

the chain length effect on the efficiency of the TIGER2/TIGER3 method is insignificant.

From the 30 ns calculation based on the dense-phase model of the C_{96} PE melt, the calculated characteristic ratio, $\langle R^2\rangle/(N-1)l^2$, and the ratio of $\langle R^2\rangle/\langle R_G{}^2\rangle$ at 400 K are 6.535 and 6.220, respectively. These values are in very reasonable agreement with the theoretical predictions of $\langle R^2\rangle/(N-1)l^2 = 6.7$ for an equilibrated PE melt and $\langle R^2\rangle/\langle R_G{}^2\rangle = 6.0$ for equilibrium Gaussian chains.[16,42] The intermolecular pair distribution function calculated by eq 4 is plotted in Figure 8. The distributions of the peaks corresponding to the nearest-neighbor and next-nearest-neighbor interchain distance are in very good agreement with the result of Smith et al. for C_{44} PE at 400 K (Figure 1 in ref 18). Since the TIGER2/TIGER3 simulation used a higher molecular weight model of PE, the peaks in the TIGER2/TIGER3 profile are sharper and higher than those in ref 18, and the peak at the third nearest distance is more distinct than that in ref 18. We also calculated the total pair distribution function including both intermolecular and intermolecular contributions and then calculated the static scattering factor, $S(q)$, based on eq 5. The calculated profile of $S(q)$ is shown in Figure 9 along with the X-ray diffraction data of C_{6400} PE at 430 K.[20] The TIGER2/TIGER3 simulation result agrees very well with the experimental data as well as the Monte Carlo simulation result of Uhlherr et al. (Figure 4 in ref 19) for C_{1000} PE at 450 K. Figure 10 plots the profiles of the weighted intermolecular orientational correlation function, $s(r)g_v(r)$, for two-bond segments. Again, the TIGER2/TIGER3 results for $s(r)$ agree very well with the results of Smith et al. (Figure 2 in ref 18). The peaks in the TIGER2/TIGER3 profiles become shaper and higher than the results of the smaller molecular weight (C_{44}) model given by Smith et al. In addition, the presence of the peak at the forth nearest distance in the TIGER2/TIGER3 profile is more significant than that in the profile given in ref 18.

TIGER2/TIGER3 Comparison with TIGER2 Alone. Figure 11 compares the temporal evolutions of potential energy of the sampled baseline temperature level states obtained from 140 ns TIGER2 and TIGER2/TIGER3 simulations using the CG model of PMMA. It shows that the potential energy resulting from the TIGER2/TIGER3 scheme dropped rapidly in a very short time after the simulation started and that the overall potential energy

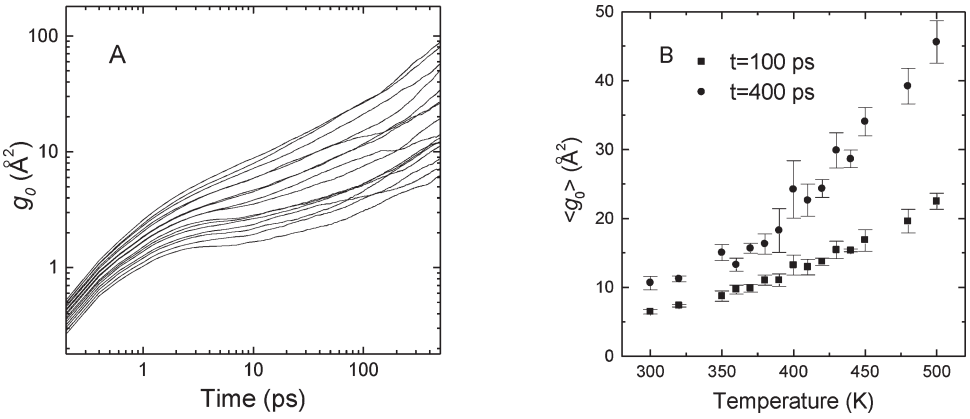

Figure 12. TIGER2/TIGER3 results of (A) change of MSDs following with time at different temperatures and (B) MSDs as a function of temperature at two observation times. Two diffusion regimes can be identified at temperatures about 390−400 K, from which the glass transition temperature can be estimated for PMMA.

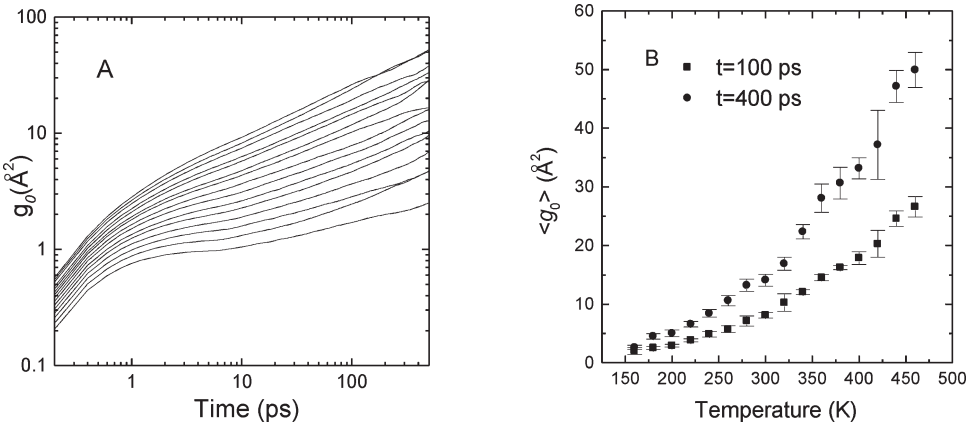

Figure 13. TIGER2/TIGER3 results of (A) change of MSDs following with time at different temperatures and (B) MSDs as a function of temperature at two observation times. Two diffusion regimes can be identified at temperatures about 290−300 K, from which the glass transition temperature can be estimated for PBMA.

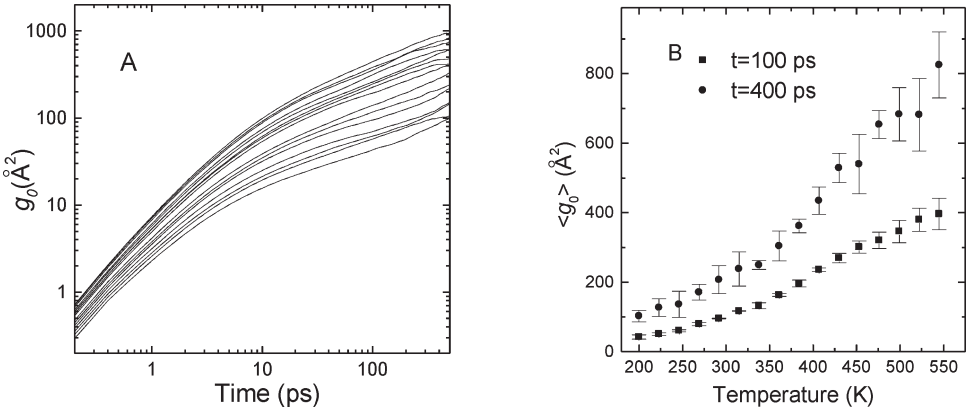

Figure 14. TIGER2/TIGER3 results of (A) Change of MSDs following with time at different temperatures and (B) MSDs as a function of temperature at two observation times. Two diffusion regimes can be identified at temperatures about 330−340 K, from which the glass transition temperature can be estimated for DTBS.

of the sampled states obtained from the mixed sampling scheme was consistently lower than that obtained from the TIGER2 method alone. These results indicate that the mixed scheme of TIGER2/TIGER3 provides more efficient sampling than the TIGER2 scheme by itself in exploring the phase space and equilibrating the bulk-phase models of amorphous PMMA.

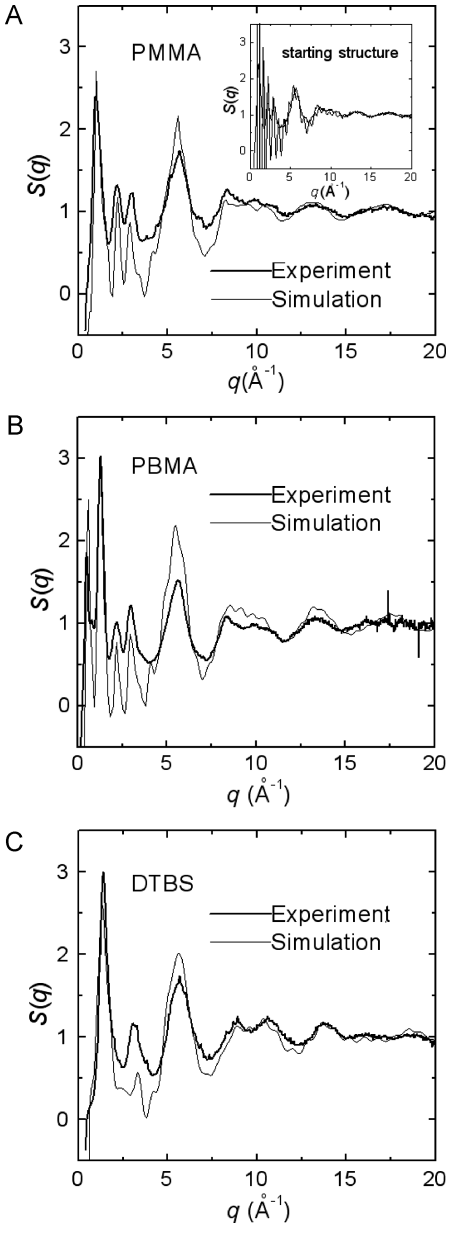

Figure 15. The structure factor, S(q), for (A) PMMA, (B) PBMA, and (C) DTBS, obtained from experiments (bold line) and simulations (light line) at 295 K temperature. Inset of plot (A) provides $S(q)$ for the PMMA polymer model prior to conducting the TIGER2/TIGER3 simulations with comparison to the experimental data.

Calculation of T_g and $S(q)$ and Comparison with Experimental Measurements. The time dependences of MSD (or $g_0(t)$ given by eq 7) were analyzed for all beads at 12 temperatures ranging evenly spaced from 250 to 550 K for PMMA, from 150 to 450 K for PBMA, and from 200 to 550 K for DTBS, and the results over each respective temperature range for PMMA, PBMA, and DTBS are plotted in Figures 12A, 13A, and 14A, respectively. Similar to the prediction made by Tsige and Taylor,[38] in every plot, the profile of $g_0(t)$ contains two regions, corresponding to the ballistic region, during which $g_0(t)$ grows as t^2, and the diffusive region, during which the growth of $g_0(t)$ does not follow a well-defined power law. At a given simulation time, the diffusive region rises monotonically as temperature rises. To estimate T_g, three independent molecular dynamics simulations were conducted, and then the averaged value of $\langle g_0 \rangle$ and the corresponding standard deviation were calculated for each temperature at different observation times. The changes of $\langle g_0 \rangle$ with temperature at two simulation times (t = 100 ps and t = 400 ps) are plotted in Figures 12B, 13B, and 14B for PMMA, PBMA, and DTBS, respectively. For each polymer, $\langle g_0 \rangle$ is proportional to temperature, but in the profiles of $\langle g_0 \rangle$ as a function of temperature for the two different observation times, there is a distinct change in slope that occurs around the same temperature. The change happens about 390−410 K for PMMA, 290−310 K for PBMA, and 330−350 K for DTBS and physically corresponds to the temperature that provides sufficient thermal energy for the polymer chains to transition from a glassy to a rubbery state. These temperatures are thus identified to be the glass temperatures for the three polymers. The polymer chain segments are more diffusive when temperature increases across T_g, leading to the greater fluctuation of $\langle g_0 \rangle$ (or larger standard deviations in statistics). The calculated values of T_g are in very good agreement with the experimental values of 397,[21] 300,[22] and 340 K for PMMA, PBMA, and DTBS, respectively.

To compare the calculated profiles of $S(q)$ with those measured experimentally by X-ray diffraction, the simulation results of $S(q)$ are plotted together with the corresponding experimental results, as shown in Figure 15 for PMMA, PBMA, and DTBS. The location of each peak pertains to a specific structural feature in the bulk amorphous polymer, with each of these three polymers revealing a distinctly different set of peak locations. For PMMA, the $S(q)$ profile of the starting structure is also plotted as an inset. As evident from the starting structure of PMMA that was obtained before the TIGER2/TIGER3 method was applied, the $S(q)$ profile deviates very much from the experimental data for q values ranging from 0 to 5 Å^{-1}, thus showing that this represents a non-equilibrated polymer model. However, after 140 ns of simulation using the TIGER2/TIGER3 method, the positions of the main peaks predicted for the PMMA simulation agree very well with those measured experimentally over the entire range of q. Similar close agreement is shown for the plots of PBMA and DTBS, thus validating that the TIGER2/TIGER3 method was able to generate all-atom models that realistically contained each of the primary structural features of these three amorphous polymers.

CONCLUSION

Bulk-phase models of three amorphous polymers, PMMA, PBMA, and DTBS, have been constructed in this work. The ability of the CG models combined with the mixed TIGER2/TIGER3 scheme to relax the bulk-phase model of the amorphous polymers has been demonstrated. The CG model of a polymer chain enables the general structural characteristics of the chain to be represented but functions in a manner that greatly reduces the number of degrees of freedom in the system. The mixed TIGER2/TIGER3 method then greatly accelerates the relaxation of dense, entangled systems. In the mixed scheme, the TIGER3 algorithm enables the system configuration to rapidly equilibrate to its theta solvent-like structure by setting the VDW radii of the CG beads to zero, which allows the chain segments to freely pass through one another and take on a random-coil structure, while the TIGER2 algorithm is used to efficiently relax and re-equilibrate the system following the TIGER3 process to eliminate effects caused by chain overlaps as the radii are returned to their normal size. The TIGER2/TIGER3 scheme enables the

CG polymer models to be readily used to generate equilibrium dense-phase CG representations of the amorphous bulk polymer in an efficient manner, with reverse-mapping then applied to translate the CG models back into atomistic representations of the system to provide representative equilibrated, dense-phase, atomic models of the amorphous polymer.

The effectiveness of the TIGER2/TIGER3 scheme was demonstrated by its ability to provide faster exploration of the phase space and result in the sampling of lower potential energy states than was obtained with a TIGER2 simulation alone following the same general cycling protocol. Furthermore, the ability of the combined TIGER2/TIGER3 method to provide an approximate Boltzmann-weighted ensemble of states was demonstrated by comparing simulation results with REMD results for the distributions of torsional angles and potential energy of simple models of a C_{64} PE chain. Finally, the ability of the TIGER2/TIGER3 algorithm to generate realistic models of bulk amorphous polymer structure was demonstrated by showing close agreement between the calculated T_g and $S(q)$ structural parameters with experimental results. In particular, the excellent agreement between the simulation and experimental results for $S(q)$ over the whole q spectrum of peak locations indicates that the simulation methods developed in this work are able to provide equilibrated models of amorphous polymers that accurately represent their actual molecular structures.

The present work thus provides molecular modeling methods that can be used to produce accurate dense-phase all-atom models of complex amorphous polymers. These methods can be used to explore the behavior of complex amorphous polymers and copolymers to provide a deeper understanding of how mer design and various additives may influence polymer structure and performance as well as providing realistic amorphous polymer models for investigations regarding the transport of solutes through the polymer as well as the adsorption of solutes and other molecular species to a polymer's surface for a wide-range of application-driven studies.

AUTHOR INFORMATION

Corresponding Author

*E-mail: LatourR@clemson.edu.

ACKNOWLEDGMENT

Financial support for this work was provided by RESBIO, a Research Resource funded by the National Institutes of health under NIH Grant EB001046, the New Jersey Center for Biomaterials, and Rutgers University. We also acknowledge the contributions of Dr. Pradip Biswas, Tougaloo College, Tougaloo, MS, for modifications to the CHARMM code to enable the use of the PCFF force field for polymer simulations.

REFERENCES

(1) Costache, A. D.; Ghosh, J.; Knight, D. D.; Kohn, J. *Adv. Eng. Mater.* **2010**, *12*, B3–B17.
(2) Doi, M.; Edwards, S. F. *The Theory of Polymer Dynamics*; Clarendon: Oxford, 1986.
(3) Auhl, R.; Everaers, R.; Grest, G. S.; Kremer, K.; Plimpton, S. J. *J. Chem. Phys.* **2003**, *119*, 12718.
(4) Graessley, W. W.; Hayward, R. C.; Grest, G. S. *Macromolecules* **1999**, *32*, 3510.
(5) Kamio, K.; Moorthi, K.; Theodorou, D. N. *Macromolecules* **2007**, *40*, 710–722.
(6) Tschöp, W.; Kremer, K.; Batoulis, J.; Bürger, T.; Hahn, O. *Acta Polym.* **1998**, *49*, 61–74.
(7) León, S.; van der Vegt, N.; Delle Site, L.; Kremer, K. *Macromolecules* **2005**, *38*, 8078–8092.
(8) Hess, B.; León, S.; van der Vegt, N.; Kremer, K. *Soft Matter* **2006**, *2*, 409–414.
(9) Srinivas, G.; Discher, D. E.; Klein, M. L. *Nature Mater.* **2003**, *3*, 638–644.
(10) Reith, D.; Meyer, H.; Müller-Plathe, F. *Macromolecules* **2001**, *34*, 2335–2345.
(11) Milano, G.; Goudeau, S.; Müller-Plathe, F. *J. Polym. Sci., Part B: Polym. Phys.* **2005**, *43*, 871–885.
(12) Li, X.; Latour, R. A.; Stuart, S. J. *J. Chem. Phys.* **2009**, *130*, 174106: 1–9.
(13) Li, X.; Latour, R. A. *J. Comput. Chem.* **2011**, *32*, 1091–1100.
(14) Metropolis, N.; Rosenbluth, A. W.; Rosenbluth, M. N.; Teller, A. H.; Teller, E. *J. Chem. Phys.* **1953**, *21*, 1087–1092.
(15) Curcó, D.; Alemán, C. *J. Chem. Phys.* **2003**, *119*, 2915–2922.
(16) Flory, P. J. *Principles of Polymer Chemistry*; Cornell University Press: Ithaca, NY, 1953.
(17) Manousiouthakis, V. I.; Deem, M. W. *J. Chem. Phys.* **1999**, *110*, 2753–2756.
(18) Smith, G. D.; Yoon, D. Y.; Zhu, W.; Ediger, M. D. *Macromolecules* **1994**, *24*, 5563–5569.
(19) Uhlherr, A.; Mavrantzas, V. G.; Doxastakis, M.; Theodorou, D. N. *Macromolecules* **2001**, *34*, 8554–8568.
(20) Honnell, K. G.; McCoy, J. D.; Curro, J. G.; Schwetzer, K. S.; Narten, A. H.; Habenschuss, A. *J. Chem. Phys.* **1991**, *94*, 4659–4662.
(21) Ute, K.; Miyatake, N.; Hatada, K. *Polymer* **1995**, *36*, 1415–1419.
(22) Wise, D. l.; Trantolo, D. J.; Altobelli, D. E.; Yaszemski, M. J.; Gresser, J. D.; Schwartz, E. R. *Encycl. Handb. Biomater. Bioeng., Part B: Appl.* **1995**, *1*, 104.
(23) Brooks, B. R.; Bruccoleri, R. E.; Olafson, B. D.; States, D. J.; Swaminathan, S.; Karplus, M. *J. Comput. Chem.* **1983**, *4*, 187–217.
(24) MacKerell, A. D.; Bashford, D.; Bellott, M.; Dunbrack, R. L.; Evanseck, J. D.; Field, M. J.; Fischer, S.; Gao, J.; Guo, H.; Ha, S.; Joseph-McCarthy, D.; Kuchnir, L.; Kuczera, K.; Lau, F. T. K.; Mattos, C.; Michnick, S.; Ngo, T.; Nguyen, D. T.; Prodhom, B.; Reiher, W. E.; Roux, B.; Schlenkrich, M.; Smith, J. C.; Stote, R.; Straub, J.; Watanabe, M.; Wiorkiewicz-Kuczera, J.; Yin, D.; Karplus, M. *J. Phys. Chem. B* **1998**, *102*, 3586–3616.
(25) Hariharan, P. C.; Pople, J. A. *Theor. Chim. Acta* **1973**, *28*, 213–222.
(26) Francl, M. M.; Pietro, W. J.; Hehre, W. J.; Binkley, J. S.; Gordon, M. S.; DeFrees, D. J.; Pople, J. A. *J. Chem. Phys.* **1982**, *77*, 3654–3665.
(27) Dinur, U.; Hagler, A. T. In *Reviews in Computational Chemistry*; Lipkowitz, K. B., Boyd, D. B., Eds.; VCH Publishers: New York, 1991; Vol. 2, pp 99−164.
(28) Maple, J. R.; Hwang, M. J.; Stockfisch, T. P.; Dinur, U.; Waldman, M.; Ewig, C. S.; Hagler, A. T. *J. Comput. Chem.* **1994**, *15*, 162–182.
(29) Li, X.; Latour, R. A. *Polymer* **2009**, *50*, 4139–4149.
(30) Andersen, H. C. *J. Chem. Phys.* **1980**, *72*, 2384–2393.
(31) Nosé, S. *Mol. Phys.* **1984**, *52*, 255–268.
(32) Hoover, W. G. *Phys. Rev. A* **1985**, *31*, 1695–1697.
(33) Allen, M.; Tildesly, D. *Computer Simulation of Liquids*; Oxford University Press: Oxford, 1991.
(34) Sugita, Y.; Okamoto, Y. *Chem. Phys. Lett.* **1999**, *314*, 141–151.
(35) Keen, D. A. *J. Appl. Crystallogr.* **2001**, *34*, 172–177.
(36) Lovell, R.; Windle, A. H. *Polymer* **1981**, *22*, 175–184.
(37) Chen, C.; Depa, P.; Maranasa, J. K. *J. Chem. Phys.* **2008**, *128*, 124906.
(38) Tsige, M.; Taylor, P. L. *Phys. Rev. E* **2002**, *65*, 021805.
(39) Hammersley, A. P. FIT2D V10.3 Reference Manual V4.0, European Synchrotron Radiation Facility, 1998.
(40) Qui, X.; Thompson, J. W.; Billinge, S. J. L. *J. Appl. Crystallogr.* **2004**, *37*, 678.
(41) Mo, Y. *J. Org. Chem.* **2010**, *75*, 2733–2736.
(42) Mattice, W. L.; Suter, U. W. *Conformational Theory of Large Molecules*; Wiley: New York, 1994.